Resonant x-ray reflectivity from a bromine-labeled fatty acid Langmuir monolayer

Joseph Strzalka,[1,*] Elaine DiMasi,[2] Ivan Kuzmenko,[3] Thomas Gog,[3] and J. Kent Blasie[1]
[1]*Department of Chemistry, University of Pennsylvania, Philadelphia, Pennsylvania 19104-6323, USA*
[2]*National Synchrotron Light Source, Brookhaven National Laboratory, Upton, New York 11973-5000, USA*
[3]*Complex Materials Consortium CAT, Advanced Photon Source, Argonne National Laboratory, Argonne, Illinois 60439, USA*
(Received 18 December 2003; revised manuscript received 7 September 2004; published 16 November 2004)

Resonant x-ray reflectivity exploits the energy dependence of atomic scattering factors to locate resonant atoms within the electron density distribution of thin films. We apply the technique to a monolayer of bromostearic acid at the air/water interface. The data collection protocol employed cycles through several energies in the vicinity of the bromine *K* absorption edge and verifies that the energy dependencies observed are indeed resonant effects. The analysis specifies the location of the Br atom with sub-angstrom precision and must consider both the real and imaginary parts of the changes in the scattering factor to be consistent with the known structure and stoichiometry of this test case.

DOI: 10.1103/PhysRevE.70.051603 PACS number(s): 68.18.−g, 87.16.Dg, 87.14.Cc, 87.64.Bx

I. INTRODUCTION

Langmuir monolayers provide an important interfacial system for the study of amphiphilic macromolecules of organic, bio-organic, or polymeric origin and their interactions with both polar and nonpolar atomic and molecular species. Such systems are relevant in both biomedical (e.g., biomineralization [1,2], cell membrane function, respiration [3]) and materials science (e.g., electronic and optical properties of polymeric ultrathin films [4,5]). X-ray and neutron scattering are key techniques for structural characterization of these single-monolayer systems. Specular reflectivity provides the scattering-length density (SLD) distribution of the monolayer projected onto the normal to the plane of the interface [6,7]. The SLD profile provides the overall thickness of the film, but this projection prevents the localization of particular molecular, submolecular, or atomic components of the monolayer within its profile structure unless they possess a SLD significantly different from the remainder. In neutron reflectivity, particular moieties can be located within the SLD profile by replacing ^{1}H with ^{2}H, but this requires comparison of SLD profiles for rigorously isomorphic monolayers of the unlabeled versus ^{2}H-labeled species [8,9]. In x-ray scattering, isotopic variations in scattering factors do not exist, and resonance scattering properties of the elements must be relied upon to introduce contrast variation while retaining isomorphism. Resonance (or "anomalous") x-ray diffraction is routinely employed in the structural characterization of proteins in single crystals. Although the number of resonant atoms per molecule is very small for either the native or resonant-atom-labeled protein as only heavier atoms possess a resonance in the x-ray regime, their total number in the periodic three-dimensional crystal is very large facilitating measurement of the resonance effect. Resonance x-ray reflectivity has been extensively utilized in the structural characterization of inorganic and bio-organic multilayer films on solid supports where either the density of resonant atoms within particular layers is very high, or in the case of proteins the periodicity of the multilayer otherwise provides a large total number of resonant atoms, again facilitating measurement of the resonance effect [10–14]. Single-monolayer films are much more problematic due to the low total number of resonant atoms coupled with the small magnitude of the resonant effect. There is only one reported example of a resonance x-ray reflectivity study of a single monolayer of a protein, and there the resonant effect from the protein's metal atom was enhanced through its interference with the nonresonant reflectivity from an underlying organic multilayer substrate [15]. Development of analogous resonance x-ray reflectivity techniques for the structural characterization of single Langmuir monolayers of amphiphilic macromolecules at the air/water interface would be of great value. For instance, it would open the door to localizing resonant-atom-labeled, single amino acid residues within the SLD profile of single monolayers of vectorially oriented proteins, analogous to those that can now only be performed by neutron reflectivity with ^{2}H-labeled proteins [8,9]. This requires that the alignment of the liquid surface spectrometer be precisely maintained as the x-ray energy is varied about the resonant atom's absorption edge and utilization of data analysis techniques not relying on interferometry. Furthermore, x-ray radiation damage of organic and bio-organic monolayer films may preclude accurate measurement of the resonance effect, the small total number of resonant atoms in the film requiring extensive data acquisition times for satisfactory statistics.

The first resonance scattering study of a liquid surface involved liquid metal alloys, impervious to radiation damage and containing a high mole fraction of resonant atoms [16]. Here we apply resonance reflectivity to investigate the location a resonant Br atom covalently bound to the hydrocarbon chain of an organic fatty acid in a Langmuir monolayer on the surface of water. This essential test case of known resonant atom stoichiometry and location within the chemical structure of the macromolecular species demonstrates that resonance reflectivity at the air/water interface can specify an atomic position with subangstrom precision. Our data collection protocol demonstrates the correct energy dependence of the resonance effect in the brominated sample and the ab-

*Electronic address: strzalka@sas.upenn.edu

sence of an effect in a control without Br and also verifies the absence of radiation damage to either sample. A model-independent method provided the SLD distribution from data below the resonant energy. The resonant atom location in the SLD profile was modeled, taking into account both the real and imaginary parts of the resonant scattering factor, from data near or on resonance. Neglecting the imaginary part of the resonant scattering factor leads to an incorrect result. In these respects, the present work differs from a recently reported resonant x-ray reflectivity study of the distribution of counter-ions adsorbed to the polar lipid headgroups of a phospholipid monolayer [17].

II. METHODS

Measurements were performed at Beamline 9-ID of the Complex Materials Consortium (CMC CAT) at the Advanced Photon Source, where a constant exit height monochromator can change the energy of the beam while keeping the downstream optics in alignment. The third harmonic of the undulator was detuned by 200 eV above the monochromator energy. The energy $K=K_{\mathrm{Br}}=13474$ eV was calibrated by the absorption from KBr salt as the energy was scanned. A split ion chamber monitor and feedback control of the voltage applied to the second crystal of the monochromator maintained the position of the beam at the monitor (9 m before the sample). Horizontally, the beam was slightly overfocused and diverging at the scintillation counter detector, while vertically it was unfocused. Incident slits were 2 mm wide and 50 μm high; detector slits were 2×2 mm^2. Contamination of the beam by higher harmonics was negligible. The liquid surface spectrometer (LSS) and Langmuir trough sample chamber have been previously described [18,19]. Attenuating filters of Mo foil in 50-μm steps kept the count rate <20 kHz. To prevent radiation damage, the sample was translated transverse to the x-ray beam by 40 μm between datapoints at large q_z and 2 mm between successive scans.

We spread monolayers from 1 mg/ml (≈3.5 mM) solutions of stearic acid $[\mathrm{SA},\mathrm{CH_3(CH_2)_{16}COOH}]$ or 2-bromostearic acid $[\mathrm{2BrSA},\mathrm{CH_3(CH_2)_{15}CHBrCOOH}]$ (Sigma, St. Louis, MO) in HPLC-grade chloroform onto MilliQ water subphases at 5 °C. Monolayers were compressed to and maintained at a surface pressure (π) of 5 mN/m.

III. RESULTS

Pure water serves to identify systematic energy dependencies in the measurement and normalization technique since the reflectivity from liquid/vapor interfaces is so well understood [6,20]. We treat the reflectivity $R(q_z)$ from pure water and from the monolayers by fitting the Fresnel function R_F to data points near q_c, and subsequently analyzing the Fresnel-normalized reflectivity, $R(q_z)/R_F$. For the water surface, modeled as a rough interface of finite width σ, this is described by a Gaussian: $R(q_z)/R_F=A_{\mathrm{H_2O}}\exp(-q_z^2\sigma^2)$. All the scans are well fit by the Gaussian, with very similar values for $\sigma(2.57\pm0.01$ Å), but the amplitude had a reproducible and small energy-dependent change $(1.01<A_{\mathrm{H_2O}}<1.04)$. We treat this as a systematic error introduced, perhaps, by errors in the calibration of the attenuation factors for the Mo filters. We take the average amplitude of the Gaussians for each energy, $A_{\mathrm{H_2O}}(E)$, as an empirical correction factor to normalize $R(q_z,E)/R_F$.

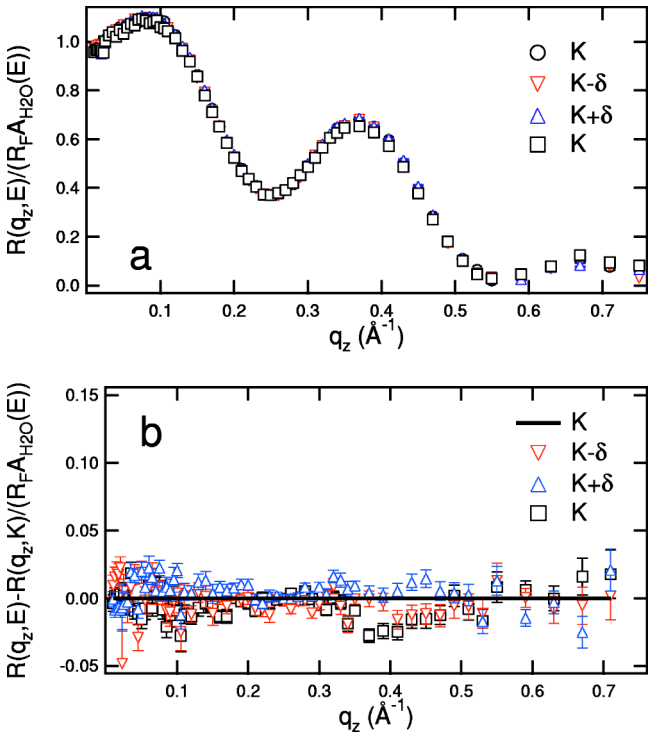

FIG. 1. (a) Fresnel- and energy-normalized reflectivity data for the control stearic acid monolayer at energies in the vicinity of the absorption edge $K=13\,474$ eV, $\delta=200$ eV. (b) Differences computed for the data in (a) and the first data set at $E=K$.

The variation in $R(q_z,E)/[R_F A_{\mathrm{H_2O}}(E)]$ from the control SA monolayer, which limits our sensitivity to resonant effects, is quite small (Fig. 1). In contrast, $R(q_z,E)/[R_F A_{\mathrm{H_2O}}(E)]$ from 2BrSA monolayers shows a definite and reproducible energy dependence (Fig. 2). The amplitudes of the two maxima are more similar for $K\pm\delta$ ($\delta=200$ eV) than for K, while the minimum near $q_z=0.3$ Å^{-1} is slightly shifted for $K-\delta$ compared to K, $K+\delta$. This general behavior can be expected from the tabulated values for the real and imaginary parts of the scattering factor, $f'(E), f''(E)$. For Br at $E=K=13\,474$ eV, $f'(K)=23.26e^-, f''(K)=3.862e^-$; at 13 274 eV, $f'(K-\delta)=30.98e^-, f''(K-\delta)=0.5449e^-$; at 13 674 eV, $f'(K+\delta)=31.39e^-, f''(K+\delta)=3.231e^-$ [21]. The change in $f'(E)$, which is approximately symmetric about the edge energy, dominates the resonant effect, consistent with the data from $K\pm\delta$ having similar amplitudes. The change in $f''(E)$ is asymmetric about the edge, resulting in the data from $K-\delta$ being slightly out of phase with those from $K, K+\delta$. The smoothly varying, reproducible data show that the monolayer withstands the radiation dose.

We can quantify the agreement between different data sets by computing the crystallographic figure of merit, the R factor. In terms of the reflectivity as the modulus squared of the structure factor of the electron density profile gradient, we have $R(q_z,E)/[R_F A_{\mathrm{H_2O}}(E)]=|F(q)|^2_{\mathrm{expt}}$ and define the R factor

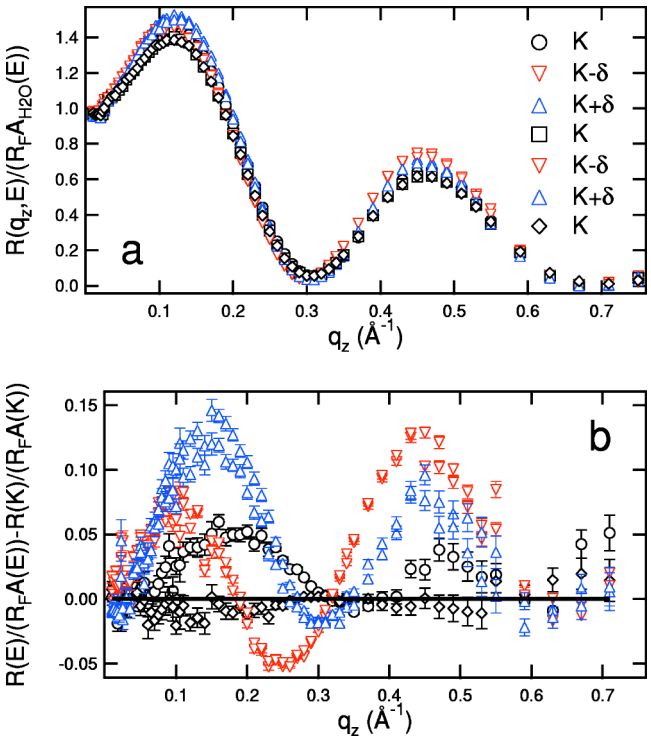

FIG. 2. (a) Fresnel- and energy-normalized reflectivity data for the 2-bromo-stearic acid monolayer at energies in the vicinity of the absorption edge $K=13\,474$ eV, $\delta=200$ eV. (b) Differences computed for the data in (a) and the second data set at $E=K$.

as $r=\Sigma(|F(q)|_{\text{expt}}-|F(q)|_{\text{model}})^2/\Sigma|F(q)|^2_{\text{expt}}$. Computing $|F(q)|_{\text{expt}}$ from the first data set at $E=K$ for the SA monolayer and using the other data sets in turn to compute $|F(q)|_{\text{model}}$ gives $r<4\times10^{-4}$. For the 2BrSA monolayer, making comparisons between the various data sets and the second data set at $E=K$ results in similar values, $r\approx6\times10^{-4}$, for the other datasets at $E=K$ but significantly larger values, $r\approx2\times10^{-3}$, for $E=K\pm\delta$.

IV. ANALYSIS

We first treat the control SA monolayer. Computing the inverse Fourier transform of $R(q_z,E)/[R_F A_{H_2O}(E)]$ gives us the autocorrelation function of the profile gradient, which indicates that the monolayer is about 30 Å thick (Figs. S2, S3 of Ref. [25]). The finite extent of the monolayer provides a powerful constraint that allows us to solve the phase problem for this structure using the iterative box refinement algorithm [22]. The box-refinement result describes the data sets nearly as well as the data set at $E=K$ describes the data sets at the other energies ($r\approx7\times10^{-4}$).

For the 2BrSA monolayer, we cannot apply box refinement directly to solve for the structure because box refinement yields a strictly real electron density distribution, while the scattering factor of Br makes the electron density distribution complex in the vicinity of the K edge. However, as the imaginary component of the scattering factor of Br is small, $E=K-\delta$, we will approximate it as zero—i.e., $f''(E=K-\delta)=0.5449e^-\approx0$. This will permit us to apply the box-refinement algorithm to the low-energy normalized reflectivity data and so obtain a numerical value for the normal derivative of the electron density distribution, $d\rho/dz(E=K-\delta)_{\text{expt}}$. Fitting a sum of Gaussians to this derivative gives us an analytical expression $d\rho/dz(E=K-\delta)_{\text{anal}}$, which closely approximates $d\rho/dz(E=K-\delta)_{\text{expt}}$ (Fig. S5 of Ref. [25]). We can then integrate this to obtain $\rho(z,E=K-\delta)_{\text{anal}}$ and Fourier transform it to obtain $F(q,E=K-\delta)_{\text{anal}}$, whose modulus squared should match the normalized x-ray reflectivity data(Fig. S6 of Ref. [25]). At the two higher energies K and $K+\delta$, the energy-dependent scattering factor of Br will be $f(E)=f(K-\delta)+\Delta f'(E)+i\Delta f''(E)$. We assume that the change in the scattering factor is distributed as a Gaussian of complex amplitude centered on the position of the resonant Br atom, z_{res}, with a finite width σ_{res}: $\rho(z,E)=\rho(z,E=K-\delta)_{\text{anal}}+\{[\Delta f'(E)+i\Delta f''(E)]/A_{\text{mol}}\}\exp[-(z-z_{\text{res}})^2/\sigma^2_{\text{res}}]$, where A_{mol} is 29.5 Å^2 for 2BrSA at $\pi=5$ mN/m. The Fourier transform of the derivative of this expression is readily computed analytically (see the Appendix of Ref. [25]) and can be compared to $R(q_z,E)/[R_F A_{H_2O}(E)]$ collected at the energies $E=K,K+\delta$, while the parameters σ_{res} and z_{res} are varied (Fig. S7 of Ref. [25]). Additionally, since the monolayer structure does not change as the x-ray energy is varied, we require consistency for the parametrers σ_{res} and z_{res} by fitting the data sets simultaneously. In this way, we determined the location of the Br atom within the 2BrSA monolayer as $z_{\text{res}}=-16.0\pm0.2$ Å, with a width of $\sigma_{\text{res}}=2.8\pm0.2$ Å.

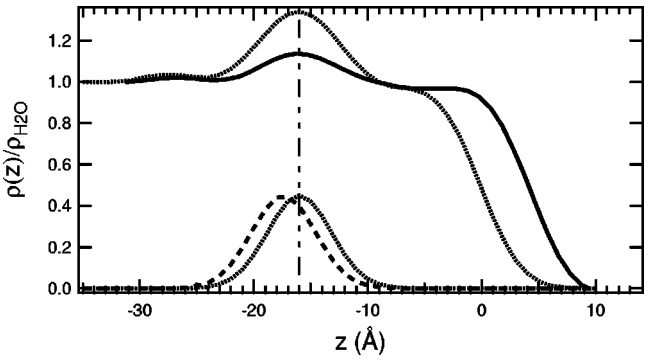

FIG. 3. Electron density profile structures for the SA (solid) and 2BrSA (upper dotted curve) monolayers from box refinement. The Gaussians at the bottom show the entire real part of the scattering factor of bromine at $E=K-\Delta(30.98e^-)$, according to the analysis that either includes the imaginary part of the resonant change in the scattering factor, $\Delta f''\neq0$ (dotted line), or neglects it, $\Delta f''=0$ (dashed line). Note that the Br atom is only coincident with the maximim in the 2BrSA profile structure when $\Delta f''$ is included.

Figure 3 superimposes the profile structures for the 2BrSA and SA monolayers as determined at $E=K-\delta$. The brominated carbon of 2BrSA is adjacent to the carboxyl headgroup effectively increasing the width and density of the headgroup feature relative to that of SA. The Br atom prevents tight packing of the 2BrSA monolayer, causing the hydrocarbon chains to tilt more and form a layer thinner than in SA. The resonance data confirm that the Br atom is at the maximum in the headgroup feature of the 2BrSA monolayer as expected since Br has the largest electron density of any atom present.

V. DISCUSSION AND CONCLUSIONS

Determination of the Br atom's location within the monolayer profile structure required simultaneous fitting of all the data available. There was not enough information present in an individual data set to obtain results for the Br position and width consistent with that from the data sets at the other energy. Therefore, in applying the technique to peptide monolayers, with Br area densities 3–10 times smaller than in 2BrSA, more information will probably be gained by collecting data sets at different energies, rather than repeating data sets at fewer energies. At least one energy must be repeated to verify that the sample is not changing with time, as radiation damage can be a problem [23].

Computing R factors demonstrates that the approximation we used to apply box refinement to the data at $E=K-\Delta$—namely, $f''=0.5449\approx 0$—was justified. Taking the 6-Gaussian fit to the box-refinement result for 2BrSA and adding in a Gaussian of width σ_{res} centered on z_{res} with an amplitude of $if''(E=K-\Delta)/A_{\mathrm{mol}}$ or $0.5449i/29.5$ Å^2 did not change the R factor significantly (0.000 744 versus 0.000 750).

In contrast, the change in the scattering factor at the higher energies relative to the $E=K-\Delta$ data set could not be treated as strictly real. The procedure presented here resulted in R factors for the fits to the $E=K,K+\Delta$ data sets of $r\approx 8\times 10^{-4}$, similar to the R factor (7×10^{-4}) for the 6-Gaussian fit to the low-energy data upon which the resonant model was based (Table S3 of Ref. [25]). However, when the data were analyzed by the same procedure but with the change in the imaginary part neglected, $\Delta f''=0$, comparable fits were obtained for the $E=K$ data $(r\approx 7\times 10^{-4})$, but not for the $E=K+\Delta$ data $(r\approx 2\times 10^{-3})$. More significantly, the Br position obtained from these fits was shifted away from the peak in the headgroup feature toward the subphase by 1.4 Å, a distance greater than the separation between carbon atoms projected onto the axis of an all *trans* alkyl chain (Fig. 3).

Our analysis rests on the published values for the change in f' and f'' for bromine (see Results) [21]. These values may be checked indirectly by treating $\Delta f''(E=K),\Delta f''(K),\Delta f''(K+\delta)$, and $\Delta f''(K+\delta)$ as floating parameters along with z_{res} and σ_{res} in a simultaneous fit of the data sets. This resulted in marginally better fits $(r\approx 6\times 10^{-4})$, a significant shift in the Br location away from the subphase $(z_{\mathrm{res}}=-14.8\pm 0.2$ Å) and a slight increase in the width of the Gaussian $(\sigma_{\mathrm{res}}=3.2\pm 0.2$ Å). The corresponding values of the scatterng factor, referenced to the tabulated values at $E=K-\delta$, are $f'(K)=24.5\pm 0.6, f''(K)=9.9\pm 1.2, f'(K+\delta)=32.8\pm 1.3$, and $f''(K+\delta)=8.0\pm 0.4$, which suggest that the imaginary part of the resonant effect for this system might be larger than expected. We did not attempt the extended x-ray absorption fine structure (EXAFS) scan of the monolayer necessary for direct determination of the $\Delta f',\Delta f''$ values from the sample [24], due to the difficulties involved in maintaining alignment of the spectrometer as the incident energy is changed.

This study demonstrates the feasibility of resonance x-ray reflectivity measurements on Br-labeled Langmuir monolayers with what we think are approaches to the data collection and analysis required to obtain the most reliable information regarding the location of the resonant species. A best-practice approach would also measure the change in f' and f'' directly from the sample and constrain the location of the resonant atoms even further.

ACKNOWLEDGMENTS

This work was supported by the NIH under Grant No. GM-55876 and by the MRSEC program of the NSF under Award No. DMR96-32598. Use of the Advanced Photon Source was supported by the U.S. Department of Energy, Office of Science, Office of Basic Energy Sciences, under Contract No. W-31-109-Eng-38.

[1] S. Mann, B. R. Heywood, S. Rajam, and J. D. Birchall, Nature (London) **334**, 692 (1988).
[2] S. Mann, Nature (London) **646**, 499 (1993).
[3] J. A. Zasadzinski, J. Ding, H. E. Warriner, F. Bringezu, and A. J. Waring, Curr. Opin. Colloid Interface Sci. **6**, 506 (2001).
[4] H. Baltes, M. Scwendler, C. A. Helm, R. Heger, and W. A. Goedel, Macromolecules **30**, 6633 (1997).
[5] M. S. Kent, Macromol. Rapid Commun. **21**, 243 (2000).
[6] J. Als-Nielsen, D. Jacquemain, K. Kjaer, F. Leveiller, M. Lahav, and L. Leiserowitz, Phys. Rep. **246**, 251 (1994).
[7] M. Lösche, *Peptide-Lipid Interactions*, Current Topics in Membranes (Academic, San Diego, 2002), p. 117ff.
[8] J. K. Blasie and P. Timmins, MRS Bull. **24**, 40 (1999).
[9] J. Strzalka, B. G. Gibney, S. K. Satija, and J. K. Blasie, Phys. Rev. E (to be published).
[10] J. Stamatoff, P. Eisenberger, J. K. Blasie, J. M. Pachence, A. Tavormina, M. Erecinska, P. L. Dutton, and G. Brown, Biochim. Biophys. Acta **679**, 177 (1982).
[11] J. K. Blasie, J. M. Pachence, A. Tavormina, M. Erecinska, P. L. Dutton, J. Stamatoff, P. Eisenberger, and G. Brown, Biochim. Biophys. Acta **679**, 188 (1982).
[12] J. K. Blasie, J. M. Pachence, A. Tavormina, P. L. Dutton, J. Stamatoff, P. Eisenberger, and G. Brown, Biochim. Biophys. Acta **723**, 350 (1983).
[13] R. H. Fairclough, R. C. Miake-Lye, R. M. Stroud, K. O. Hodgson, and S. Doniach, J. Mol. Biol. **189**, 673 (1986).
[14] F. J. Asturias and J. K. Blasie, Biophys. J. **59**, 488 (1991).
[15] J. M. Pachence, R. F. Fischetti, and J. K. Blasie, Biophys. J. **56**, 327 (1989).
[16] E. DiMasi, H. Tostmann, O. G. Shpyrko, P. Huber, B. M. Ocko, P. S. Pershan, M. Deutsch, and L. E. Berman, Phys. Rev. Lett. **86**, 1538 (2001).
[17] D. Vaknin, P. Krüger, and M. Lösche, Phys. Rev. Lett. **90**, 178102 (2003).
[18] A. H. Weiss, M. Deutsch, A. Braslau, B. M. Ocko, and P. S. Pershan, Rev. Sci. Instrum. **57**, 2554 (1986).
[19] A. Braslau, P. S. Pershan, G. Swislow, B. M. Ocko, and J. Als-Nielsen, Phys. Rev. A **38**, 2457 (1988).

[20] H. Tostmann, E. DiMasi, P. S. Pershan, B. M. Ocko, O. G. Shpyrko, and M. Deutsch, Phys. Rev. B **59**, 783 (1999).
[21] B. L. Henke, E. M. Gullikson, and J. C. Davis, At. Data Nucl. Data Tables **54**, 181 (1993), http://www.cxro.lbl.gov/optical_constants/pert_form.html
[22] J. K. Blasie, S. Zheng, and J. Strzalka, Phys. Rev. B **67**, 224201 (2003).
[23] R. Edgar *et al.*, J. Phys. Chem. B **104**, 6843 (2000).
[24] J.-L. Hodeau *et al.*, Chem. Rev. (Washington, D.C.) **101**, 1843 (2001).
[25] See EPAPS Document No. E-PLEEE8-70-099411 for supporting information, including seven figures and an appendix showing the expression for the sum of Gaussians used to fit the data. A direct link to this document may be found in the online article's HTML reference section. The document may also be reached via the EPAPS homepage (http://www.aip.org/pubservs/epaps.html) or from ftp.aip.org in the directory /epaps/. See the EPAPS homepage for more information.